

Optofluidic solar concentrators using electrowetting tracking: Concept, design, and characterization

Jiangtao Cheng^{a,*}, Sungyong Park^b, Chung-Lung Chen^{b,1}

^a Department of Mechanical and Energy Engineering, University of North Texas, Denton, TX 76207, United States

^b Teledyne Scientific Company, 1049 Camino Dos Rios, Thousand Oaks, CA 91360, United States

Received 27 August 2012; received in revised form 24 November 2012; accepted 21 December 2012

Available online 30 January 2013

Communicated by: Associate Editor Yanjun Dai

Abstract

We introduce a novel optofluidic solar concentration system based on electrowetting tracking. With two immiscible fluids in a transparent cell, we can actively control the orientation of fluid–fluid interface via electrowetting. The naturally-formed meniscus between the two liquids can function as a dynamic optical prism for solar tracking and sunlight steering. An integrated optofluidic solar concentrator can be constructed from the liquid prism tracker in combination with a fixed and static optical condenser (Fresnel lens). Therefore, the liquid prisms can adaptively focus sunlight on a concentrating photovoltaic (CPV) cell sitting on the focus of the Fresnel lens as the sun moves. Because of the unique design, electrowetting tracking allows the concentrator to adaptively track both the daily and seasonal changes of the sun's orbit (dual-axis tracking) without bulky, expensive and inefficient mechanical moving parts. This approach can potentially reduce capital costs for CPV and increases operational efficiency by eliminating the power consumption of mechanical tracking. Importantly, the elimination of bulky tracking hardware and quiet operation will allow extensive residential deployment of concentrated solar power. In comparison with traditional silicon-based photovoltaic (PV) solar cells, the electrowetting-based self-tracking technology will generate ~70% more green energy with a 50% cost reduction.

© 2013 Elsevier Ltd. All rights reserved.

Keywords: Electrowetting on dielectric; Optofluidics; Adaptive solar tracking; Dual-axis tracker; Solar concentrator

1. Introduction

Solar radiation accounts for most of the available renewable energy on earth. To harvest solar energy, the most common way is to use solar panels with photovoltaic (PV) solar cells or concentrating photovoltaic (CPV) solar cells for solar energy conversion (Luque and Andreev, 2007; Neufeld et al., 2008). Solar PV panels, throughout their entire existence, have had the same issue over and over again: solar cells can generate more power when sun-

light is perpendicular to the panel; once the sun's light begins to hit solar cells with an angle, they become less efficient, so fixed solar panels are only efficient at noon (Roth et al., 2004). Soon after people realized that, they began constructing all sorts of solar trackers that can track the movement of the sun across the sky and would correspondingly modify the panels' position so as to face the sun directly (Rubio et al., 2007). Because of their ability to constantly face the sun, solar panels having a tracking system are 40% more efficient than a fixed, single axis solar system and can nearly double the energy output (2×) of solar panels (Huang et al., 2011).

Concentrating photovoltaic (CPV) systems convert sunlight energy into electricity in the same way as conventional PV technology does (Kurtz, 2011). Current III–V junction

* Corresponding author. Tel.: +1 940 369 5929; fax: +1 940 369 8675.

E-mail address: Jiangtao.Cheng@unt.edu (J. Cheng).

¹ Present address: Department of Mechanical and Aerospace Engineering, University of Missouri, Columbia, MO 65211, United States.

Nomenclature

γ_{IJ}	the surface tension between phase I and phase J	D	the aperture size of the fluid
θ_Y	the liquid contact angle with no voltage applied	n	the refractive index of the liquid
C	the unit area capacitance of the dielectric layer	α	the incident angle of light
d	the dielectric thickness	θ	the tilt angle of the fluid interface
ε	the dielectric constant	β	the refraction angle
V	the applied voltage	t	the critical damping time on a fluid surface
ρ	the fluid density		

CPV cells are more efficient than traditional silicon-based PV cells (40% versus 15–19%). But these high-efficiency CPV cells are much more expensive than PV cells so that optical concentrators are needed to reduce the amount of III–V cells required. Consequently, incorporating an optical condenser into the CPV system can focus a large area of sunlight onto each CPV cell while providing reduced energy costs and improved manufacturability and reliability. Similar to PV panel system, the solar concentrator needs a tracking system in order to stay in line with the sun for high-efficiency solar energy harvesting.

On most of the conventional motor-driven solar tracker systems, there are mechanical moving parts. In particular, these tracker systems have an obviously increased mechanical complexity because each solar panel consists of solar concentrators, PV or CPV cells, heavy passive heat sinks or active cooling plates (Mousazadeh et al., 2009). Therefore, a mechanical tracking system is not only power hungry but also not cost effective due to the significant power consumption in tracking operations and the huge maintenance cost. In addition, even though tracking solar panels can collect more energy than stationary ones at the expense of tracking costs and additional power consumption, they are not suitable for roof-top applications because of their heavy and moving bulky structures.

Recently, there have been reported various solar concentrators without needing to mechanically track the sun. Pender (2005) patented his motion-free tracking solar concentrator that is comprised of a beam deflector and a fixed optical condenser. The one-dimensional beam deflector consists of a pair of prism arrays made of liquid crystal whose refractive index can be varied by applying an electric field. The intensity and distribution of the applied field modulates the refractive index of the individual prisms in order to keep the direction of the deflected beam fixed as the incident beam shifts. Currie et al. (2008) developed organic solar concentrators that are planar waveguides with light absorbed by the thin-film organic coating on the substrate surface. Due to the near-field energy transfer, solid-state solvation, and phosphorescence, their organic solar system gives rise to 10-fold increase of power output. However, the durability of the coated surface still needs to be further improved as field tests indicated that the performance of the organic concentrators was only stable for 3 months. In general, organic coatings require strong adhe-

sion forces between the coating materials and the substrate, and are difficult for long term maintenance. Kotsidas et al. (2011) presented nominally stationary high-concentration solar concentrators based on gradient-index lenses, which enable daylong averaged flux concentration levels of order of 10^3 . Owing to the high fabrication cost of gradient lens and the difficulties in lens scaling up, this technique is not taken as cost-effective. Baker et al. (2012) proposed a planar micro-optic solar concentrator incorporating a waveguide cladding with a nonlinear optical response to sunlight. In their optical system, the voltage-induced refractive index modulation of nanoparticle dispersions is used for self-tracking purpose that can reduce mechanical tracking requirements. Their initial experimental work with aqueous polystyrene has demonstrated a 0.033 local change of index in response to a 2 Vrms 60 Hz square wave signal indicating that an optimized material system is necessary in order to achieve the required index response.

In this paper, we introduce a novel optofluidic solar concentration system with electrowetting-on-dielectric (EWOD) tracking. The EWOD effect controls the contact angle between an electrolyte and a dielectric surface through the application of an electric field between them (Lee et al., 2002; Mugele and Baret, 2005; Jones, 2005). EWOD has been widely used in various fields such as chip-level spot cooling (Cheng and Chen, 2010a,b), adjustable liquid lens (Kuiper and Hendriks, 2004; Murade et al., 2011), clinical diagnostics (Srinivasan et al., 2004), and electronic paper (Hayes and Feenstra, 2003). Recently, there have appeared electrowetting-based micropisms for optical membrane manipulation and beam steering (Smith et al., 2006; Hou et al., 2007). However, the reported liquid prisms either have relatively small aperture sizes (from hundreds of microns to 5 mm) that constrain its real implementation or lack of successive beam tracking capabilities. In this work, we describe the operation mechanisms of an EWOD-controlled liquid prism with an aperture size as large as $10\text{ mm} \times 10\text{ mm}$ and introduce its optofluidic characteristics. Driven by a custom-built control system, the liquid prism can adaptively track an incident beam and agilely steer the beam to the desired direction. Consequently the liquid prism can work as an electrowetting solar module for adaptive solar tracking. Importantly, with their self-tracking capability, the full-field-of-view liquid prisms can more efficiently carry out solar tracking and

sunlight steering obligations without any mechanical moving structures. Our optofluidic concentration system will integrate electrowetting-based liquid prism tracking technique with an optical condenser (Fresnel lens), resulting in a wide tracking range for maximum energy generation. Key features of the optofluidic solar concentrator include adaptive and dual-axis sun tracking, no mechanical moving parts, low-power consumption, low profile and compact design and quiet operation.

2. Electrowetting solar modules

We have designed and fabricated an electrowetting-based liquid prism, i.e., electrowetting solar module as shown in Fig. 1. The geometry of the liquid prism module was designed to be 10 mm × 10 mm × 18 mm, and its weight was 20–25 g. The fabrication of the liquid prism module is summarized as the following. We diced an ITO (In₂O₃:SnO₂) glass substrate ($R_{\square} \sim 20 \Omega$) into four pieces of 10 mm × 18 mm each, which work as the module sidewalls. Ti/Au (5 nm/20 nm) contact pads were electron-beam deposited on the top and bottom ends of each ITO slide. For control signal input, four copper wires were silver epoxied (TRA-DUCT 2902) to the Ti/Au contact pads respectively. Then we applied UV epoxy (Norland ultra violet sealant 91) to assemble the four rectangular ITO sheets together to form an open square channel. Working as the adhesion promoter for parylene C, a dish of Silane A-174 (Merck KGaA) was heated below the epoxied channel for 5 min. We blew the parts off with N₂ gas to remove extra A-174 on the sidewall surfaces. Subsequently we conformally coated $\sim 1\text{-}\mu\text{m}$ -thick parylene C (or parylene HT with long-term UV stability) on the channel surface. The glass channel was then dip coated with a thin layer of flu-

oropolymer (FluoroPel™ PFC1601 V, Cytonix Corporation). After baking at 140 °C in an oven for 6 h, the surface energy of the sidewall was $\sim 16 \text{ mN/m}$. Water has a contact angle as large as $\sim 120^\circ$ on the hydrophobic sidewalls. Subsequently, the open channel was epoxied to an ITO glass substrate to form a transparent cuvette. To make the module sealed, another glass slide was attached on top.

Fig. 1 shows the detailed sidewall structure (not in scale) of the liquid prism module. The top and bottom surfaces were coated to be anti-reflective to reduce reflection loss. Then we filled the module with two immiscible fluids, e.g., water and silicone oil or optical fluid SL-5267 (Santolubes™). By applying different voltages to each wall while grounding the ITO substrate, we can modify the wettability of the walls and modulate the orientation of the fluid–fluid interface. For a liquid prism, gravity-induced interface deformation and stability are a concern especially at tilted orientations. We can overcome the deformation by synthesizing two fluids of equal density but with differing refractive indices (RIs). Thus, the prism can be maintained independent of its orientation and is rather resistant to mechanical vibration and shock (Kuiper and Hendriks, 2004). In this work, we used silicone oil (Clearco Product Co., 63148-62-9) as the high RI fluid (RI = 1.54, 0.96 g/cm³ at 20 °C) and water as the low RI fluid (RI = 1.33, 0.998 g/cm³ at 20 °C). Importantly, silicone oil has very stable physical and chemical properties and can work properly from -40°C to 280°C without apparent property degradation.

For parallel light beam (sunlight beam) deflection and steering purpose, we need to maintain the fluid–fluid interface as flat as possible. Consequently specific voltages are needed on the sidewall electrodes. As we know, the balance of the interfacial surface tensions near the water (W), oil (O), fluoropolymer (F) tri-junction line is governed by the following equations (Mugele and Baret, 2005):

$$\begin{aligned} \gamma_{WF} &= \gamma_{FO} - \gamma_{WO} \cos \theta_Y \\ \gamma_{WF}(V) &= \gamma_{WF}(0) - \frac{1}{2} CV^2 \end{aligned} \quad (1)$$

where γ_{IJ} is the surface tension between phase I and phase J, θ_Y is the water contact angle with no voltage applied, $C = \epsilon_0 \epsilon_r / d$ is the unit area capacitance of the hydrophobic dielectric, d is the dielectric thickness, $\epsilon = \epsilon_0 \epsilon_r$ is the dielectric constant and V is the applied voltage on sidewall electrodes. Therefore, when water has a contact angle θ_R on the right sidewall due to voltage V_R , the contact angle on the left sidewall needs to be $180^\circ - \theta_R$ so as to form a flat interface. According to the electrowetting relationships on both the left and the right sidewalls (Jones, 2005):

$$\begin{aligned} \cos \theta_R &= \cos \theta_Y + \frac{\epsilon V_R^2}{2d\gamma_{WO}} \\ \cos(180^\circ - \theta_R) &= \cos \theta_Y + \frac{\epsilon V_L^2}{2d\gamma_{WO}} \end{aligned} \quad (2)$$

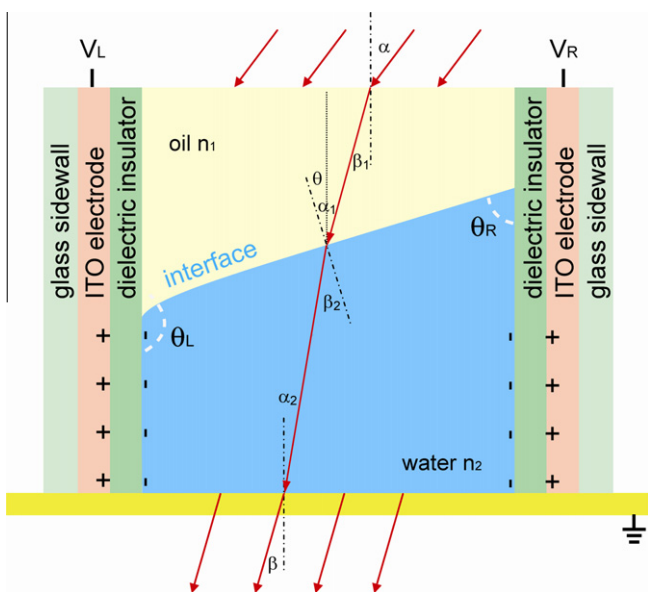


Fig. 1. Cross-sectional view of electrowetting modulation of the orientation of a fluid–fluid interface. Specific voltages are applied to the sidewalls to maintain a flat interface (Cheng and Chen, 2011).

we obtain the required voltage V_L on the left sidewall for maintaining a smooth meniscus (Cheng and Chen, 2011).

To reach a certain wettability change, low voltages are desired for real EWOD implementations. Eq. (2) implies three main approaches to reducing the driving voltage:

- deposit a thin layer of dielectric material on the sidewalls,
- use high-dielectric-constant materials such as Al_2O_3 , HfO_2 , and Ta_2O_5 ,
- add surfactant into fluids to reduce the surface tension on the fluid–fluid interface, e.g., 1 wt% of ionic surfactant, sodium dodecyl sulfate (SDS), in water can reduce the surface tension from 73 mN/m to ~ 8.6 mN/m.

Accordingly we coated a layer of parylene ($\epsilon_r = 2.8$) as thin as 1.1 μm on the cuvette sidewalls. Then we filled in the cuvette the following two fluids: one is deionized (DI) water with 1 wt% of KCl and 1 wt% of SDS, the other liquid is silicone oil. Since the two fluids have different refractive indices, light passing through the EWOD module will be deflected in a specific direction controlled by the applied voltages.

When a high DC electric field is applied over a long period to an EWOD module, it would irreversibly polarize and permanently damage the dielectric layer. Alternatively, we adopted low-frequency square-wave AC voltages to drive the EWOD modules. The square-wave signals can significantly alleviate the side effects of dielectric polarization and facilitate the interface maintenance. However, we need to avoid fluid interface oscillation under AC voltages. The critical damping time t on a fluid surface is given by Kuiper and Hendriks (2004):

$$t \approx 0.3 \sqrt{\frac{\rho D^3}{\gamma}} \quad (3)$$

where ρ is the fluid density, D is the aperture size of the fluid, and γ is the surface tension. According to Eq. (3), for a water surface of 10 mm \times 10 mm with a surface tension of ~ 10 mN/m, the damping time is estimated to be 0.09 s. This damping time determines the lower limit of the frequency range without significant meniscus oscillation. On the other hand, we do not prefer high-frequency voltages (>100 Hz) because the higher the frequency, the more the power consumption will be. In this work, the frequency we used ranges from 20 Hz to 30 Hz. With the proper selection of signal form and frequency, the orientation of the liquid prism has been maintained very stable.

In general, low-frequency square-wave signals have the following advantages:

- drive the liquid prism module with low power consumption,
- mitigate dielectric charging and avoid permanent polarization of the dielectric layer,

- facilitate liquid prism modulation and help maintain the interface orientation,
- increase reliability and service life of liquid prism modules.

We further carried out optical analyses for the liquid prism. Fig. 1 shows the optical path through a liquid prism module. The refractive indices of air, oil and water are $n_{air} = 1$, n_1 , n_2 respectively. The incident angle on the top surface is α , and the tilt angle of the fluid interface is θ . Applying Snell's law to each interface, we obtain the outgoing direction of the steered beam:

- on the interface of air and liquid 1, $\sin \alpha = n_1 \sin \beta_1$, where β_1 is the refraction angle in liquid 1.
- on the interface of liquid 1 and 2, the incident angle $\alpha_1 = \beta_1 + \theta$, $n_1 \sin \alpha_1 = n_2 \sin \beta_2$, where β_2 is the refraction angle in liquid 2.
- on the interface of liquid 2 and air, the incident angle $\alpha_2 = \beta_2 - \theta$, $n_2 \sin \alpha_2 = \sin \beta$.

Based on the optical analyses, we have developed an automatic tracking algorithm to actively and adaptively track the beam source (sun's position). These optical analyses are also used for module performance prediction. Using the customer-made control system and the developed algorithm, we have achieved continuous liquid prism modulation that enables adaptive and agile tracking of the beam source's wide-range movement. Fig. 2 are the snap-

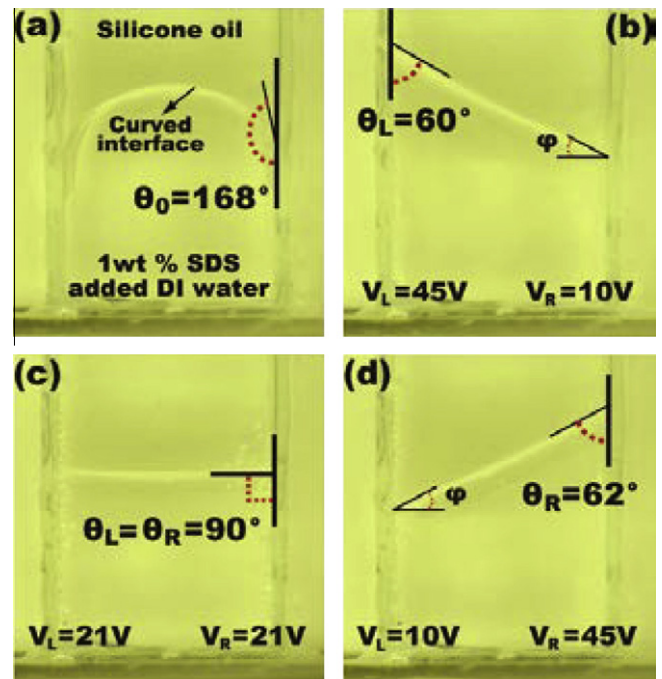


Fig. 2. Electrowetting-controlled liquid prism modulation. The tilt angle of the fluid–fluid interface is between -45° and 45° and the tracking range of incident beam is between -15° and 15° . The frequency of applied voltage is 20 Hz.

shots of the liquid prism modulation with the corresponding voltages applied to the sidewalls. As shown in Fig. 2, by applying proper voltages on the sidewalls, the water–silicone oil interface was maintained to be quite flat, the ideal profile for parallel beam deflection. Because the normal response time of electrowetting is on the order of tens of ms, no interface oscillation was observed even during the prompt electrical charging and discharging processes associated with square-wave signals. It is noteworthy that we did not observe any Rayleigh–Taylor instability on the water–silicone oil interface. This is due to fact that the density of silicone oil (0.96 g/cm^3 at $20 \text{ }^\circ\text{C}$) is very close to the water density and the Atwood number $A = (\rho_1 - \rho_2) / (\rho_1 + \rho_2) \approx 0.02$, where ρ_1 is density of heavier fluid (DI water) and ρ_2 is density of lighter fluid (silicone oil). In addition, the SDS surfactant may play an important role in the interface stability by lowering the driving voltage.

3. Optofluidic solar concentrators

The dynamic liquid prism can work as an electrowetting solar module for adaptive solar tracking and sunlight beam steering. We can arrange an array of these electro-optical modules on a large panel to form a beam steering sheet. Two or more beam steering sheets can be stacked to achieve a large steering angle ($>30^\circ$). An integrated solar concentrator can be constructed from the optofluidic beam deflector in combination with a fixed optical condenser (Fresnel lens) as shown in Fig. 3. The beam deflector consists of liquid prism arrays and electrowetting modifies the orientation of each individual liquid prism in order to steer the deflected beam normally towards the Fresnel lens as the incident sunlight beam shifts. The solar panel uses a non-reflective-coated optical acrylic Fresnel lens to capture the sunlight from an area >1000 times that of a CPV cell and focus it onto the CPV cell. Each hexagonal shaped Fresnel lens (segment) is about 5.5 in. (13.9 cm) long on each side with the solar cell located about 6 in. (152 mm) beneath the lens. Each segment is identical, so there is no scaling of this component required between various configurations. The concentration device can track the sun by

simply changing the steering direction of each electro-optical prism. Therefore, without any mechanical moving parts, the dynamic liquid prism array allows the device to adaptively track both the daily and seasonal changes of the Sun's orbit, i.e., dual-axis tracking.

The benefits of optofluidic solar concentrators are particularly significant when considering the inherent efficiency advantage of the multi-junction CPV technology over silicon PV solar cells. In high solar concentration designs, the photovoltaic cells used differ from those used in traditional photovoltaic systems which are usually crystalline silicon cells. CPV cells, referred to as “multi-junction” or “III–V” cells, provide energy conversion efficiencies much higher than traditional silicon PV cells – approximately 40% today. These high efficiencies contrast with typically 13–19% efficiency for silicon cells. With CPV designs utilizing these types of “III–V” cells, the efficiency levels of our optofluidic solar concentrators will be significantly higher than traditional PV systems. Importantly, the use of concentration allows substitution of cost-effective materials such as Fresnel lenses and fluids for the more costly semiconductor PV/CPV cell materials. This optofluidic concentration approach can reduce capital costs for CPV and increases operational efficiency by eliminating the power consumption of mechanical tracking.

4. Optical analysis of dual prism modules

As can be seen in Fig. 1, there is only one functioning fluid–fluid interface in each single prism module. Even though its tracking range can be further increased by stacking two layers of such single prism cells, however, this arrangement introduces additional energy loss due to the shadowing effect of the second layer. Alternatively we can develop a more compact module with dual prisms in each cell to accomplish significant sunlight refraction. As shown in Fig. 4, there are two functioning fluid–fluid interfaces in each dual prism module and the matching densities between the two fluids can enhance dual prism stability without gravity-induced deformation (Kuiper and Hendriks, 2004). Compared to two single prism modules stacked

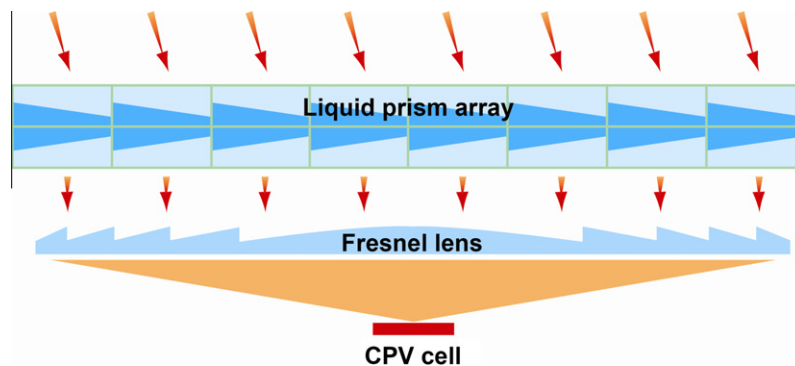


Fig. 3. Stacked liquid prism modules for significant sunlight steering. via electrowetting tracking, the optofluidic system can adaptively focus sunlight on a CPV cell sitting on the focus of the Fresnel lens as the sun moves.

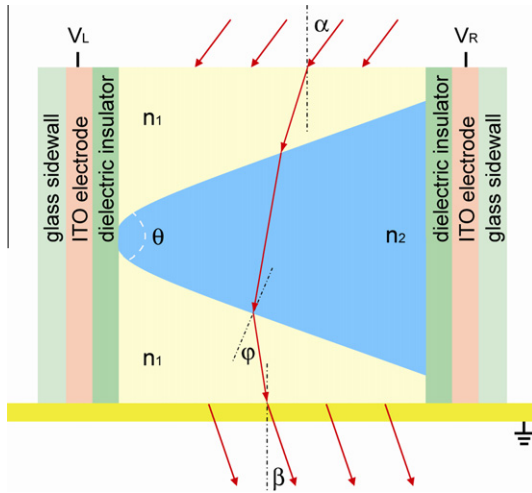


Fig. 4. Optical path inside a dual prism module. Dual interfaces can achieve a large steering angle ($\alpha > 30^\circ$).

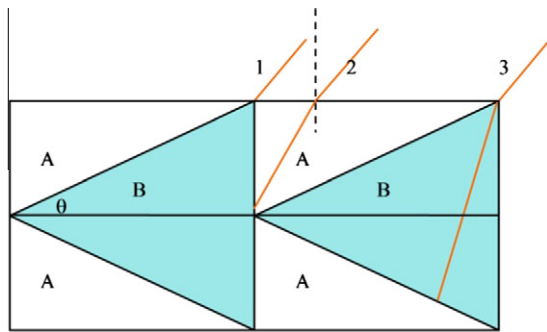


Fig. 5. Dual prism modules for significant sunlight refraction with less energy loss.

together, the dual prism configuration can reduce the shadowing effect of the sidewalls and mitigate reflection energy loss due to the fact that fewer surfaces exist through the optical path. We carried out performance analysis for dual prism modules in an arrayed configuration. In the two laterally-attached dual prism cells illustrated in Fig. 5, liquid A has a refractive index n_1 and liquid B has a relatively larger refractive index n_2 . Three main sources of energy loss are considered in our analysis. The first source is geometrical loss. When the sun is at an oblique angle, the sunlight between ray 1 and ray 2 hits on the side walls and is lost, while the light between ray 2 and ray 3 is deflected towards

the CPV cell underneath. This geometrical loss is proportional to the distance between ray 1 and ray 2. The second loss is due to possible damping or absorption of the sunlight as it travels through the liquid medium. The light intensity I decreases in the direction of propagation according to the relation, $I(x) = I_0 \exp[-4\pi kx/\lambda_0]$, where I_0 is the original optical intensity, λ_0 is the optical wavelength in vacuum, k is the absorption index of the medium. The coefficient of travel distance x in the above equation is also called the absorption coefficient, $K_a = 4\pi k/\lambda_0$ (Born and Wolf, 1999). However, due to the compact liquid prism module configuration, the absorption loss within a thin layer of fluids (2–4 cm) was estimated to be less than 5% in the optofluidic system. The third source of energy loss is due to surface reflections. This loss can be calculated by applying Fresnel’s formula (Eq. (4)) on each interface for s- and p-components respectively. Then the results are multiplied for all the interfaces and averaged for s- and p-components since the sunlight is not polarized.

$$R_s = \left(\frac{n_1 \cos \theta_i - n_2 \cos \theta_t}{n_1 \cos \theta_i + n_2 \cos \theta_t} \right)^2$$

$$R_p = \left(\frac{n_1 \cos \theta_t - n_2 \cos \theta_i}{n_1 \cos \theta_t + n_2 \cos \theta_i} \right)^2 \tag{4}$$

The geometrical loss and reflection loss at various situations are listed in Table 1. It can be seen that a relatively larger n_2 and antireflective (AR) coating are desired to significantly reduce energy loss. Therefore, a critical need for this optofluidic system is to develop high refractive index and density-matching liquids.

5. Dispersion effect of liquid prisms

Solar radiation has a wide spectrum distribution (mainly within 300–1800 nm) on the earth surface. The dispersion effect of liquid prisms must be taken into account in the system design. In the dual prism module sketched in Fig. 4, n_1 and n_2 indicate the low and high refractive indices respectively. The incoming light with an angle of incidence α is steered by the prism and has an outgoing angle β after traveling through the module. The outgoing angle β as a function of the refractive indices and the prism apex angle θ is expressed as:

Table 1
Geometrical loss and reflection loss analysis of EWOD cells.

n_1	n_2	Incident angle	Tilt angle θ	Geometrical loss (%)	Reflection loss (no AR) (%)	Reflection loss (AR coating) (%)
1.33	1.8	45°	33°	40	19	12
		25°	23°	14	13	5
		0°	0°	0	12	5
1.33	1.65	35°	38°	37	15	7
		30°	35°	28	12	5
		0°	0°	0	10	3

$$\sin \varphi = \frac{n_2}{n_1} \times \cos \left\{ \sin^{-1} \left[\frac{n_1}{n_2} \sin \left(\sin^{-1} \left[\frac{\sin \alpha}{n_1} \right] + \frac{\theta}{2} \right) \right] \right\} \sin \theta - \sin \left(\sin^{-1} \left[\frac{\sin \alpha}{n_1} \right] + \frac{\theta}{2} \right) \cos \theta \quad (5)$$

$$\beta = \sin^{-1} \left(n_1 \sin \left(\varphi - \frac{\theta}{2} \right) \right) \quad (6)$$

In the dispersion analysis, we choose water and optical fluid SL-5267 (SantoLubes™) as the low and high refractive index liquids respectively. And the dispersion properties of these two liquids are plotted in Figs. 6a and 6b respectively. Since the main response spectrum of most III–V multi-junction solar cells is from 400 nm to 1600 nm, the effect of dispersion is considered within this spectrum segment. As indicated in Fig. 6a, SL-5267 has a remarkably strong dispersion for the wavelength between 400 nm and 600 nm while water has less dispersion in this range as shown in Fig. 6b. Due to the strong dispersion of SL-5267, the outgoing angle β of the light is strongly wavelength-dependent, especially within the spectrum of 400–600 nm. Such angular dispersion causes spatial dispersion on the CPV solar cell.

We used Zemax (Radiant Zemax, LLC) to model the dispersion effect of the overall optical system. Fig. 7a shows the Zemax layout in which the deflected sunlight from a liquid prism was steered normally towards a Fresnel lens with a CPV cell sitting on its focus. In this configuration, Fresnel lens works as the optical condenser. The liquid prism aperture is 1" × 1", and the Fresnel lens aperture is 6" × 6" with a focal length of 6". Four representative wavelengths, i.e., 400 nm, 500 nm, 600 nm, and 1600 nm, were selected to illustrate the dispersion effect in this optical system. Since oblique incidence leads to more conspicuous dispersion in a liquid prism, the angle of incidence in the

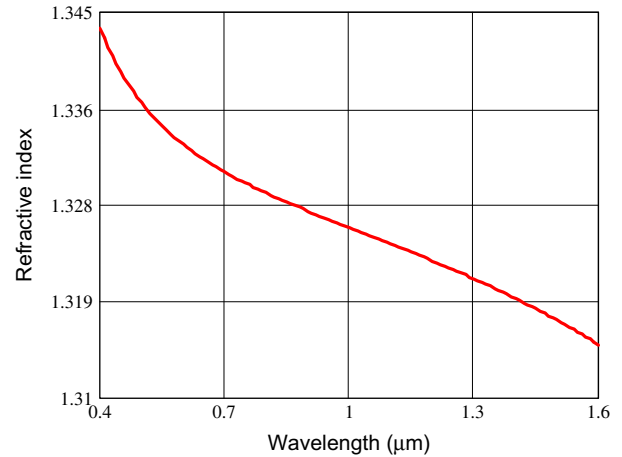


Fig. 6b. Dispersion characteristics of water.

Zemax simulation was set to be 45° corresponding to the sunlight in the early morning and in the late afternoon. According to Eqs. (5) and (6), when the light incident angle is 45°, the optimum prism apex angle θ should be modulated at 79.0° resulting in $\beta = 0^\circ$ for subsequent normal incidence on the Fresnel lens. Fig. 7b shows the spatial distribution of the focuses of various wavelengths on the CPV cell. To capture 100% optical power for all the wavelengths, the size of the solar cell should be $\geq 16 \text{ mm} \times 16 \text{ mm}$. Due to the strong dispersion at short wavelengths, more than 3/4 of the CPV area is used to collect the light of 400–500 nm, and more than 80% of the CPV area is used to collect the light of 400–600 nm under the condition of 45° light incidence. Therefore, optical liquids of low dispersion are critical to achieve both high efficiency and low cost (smaller CPV cells) purposes. CPV cell size requirement as a function of wavelength for different light incident angles is plotted in Fig. 8. According to the above dispersion analysis, cell size versus light collection efficiency tradeoff shall be performed for system design optimization. As a practical method of reducing the angular dispersion, we can overlay two liquid prisms in intimate contact but are made of materials with opposing dispersion relations (Born and Wolf, 1999).

6. Innovativeness of optofluidic solar concentrators

Besides the optofluidic solar concentration technique proposed by us, there are other two main solar energy harvesting approaches. One approach uses static and flat PV solar panels without solar tracking capability (Suntech Power, Ltd.); the other approach employs a mechanical tracking system to focus solar energy on CPV solar cells (SolFocus, Inc.). Table 2 compares the three main approaches for solar energy harvesting.

The energy conversion efficiency of traditional PV systems is typically 13–19%. So the electric power output from a 100 ft² PV panel is <2000 W. Via a motor-driven tracker system, CPV cells under concentrated light operate more

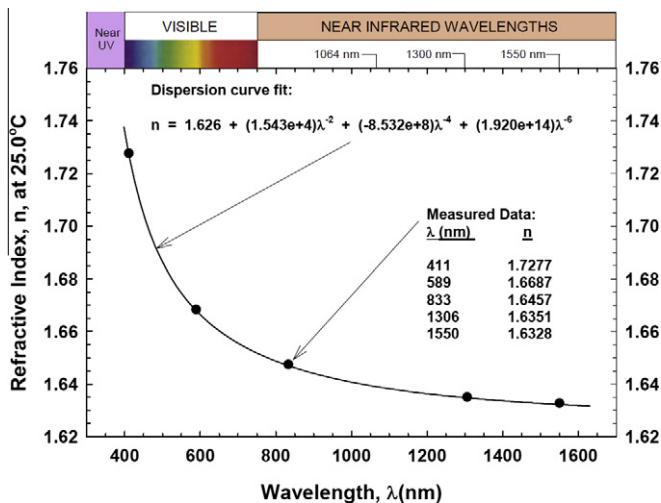


Fig. 6a. Dispersion characteristics of optical fluid SL-5267 (SantoLubes™).

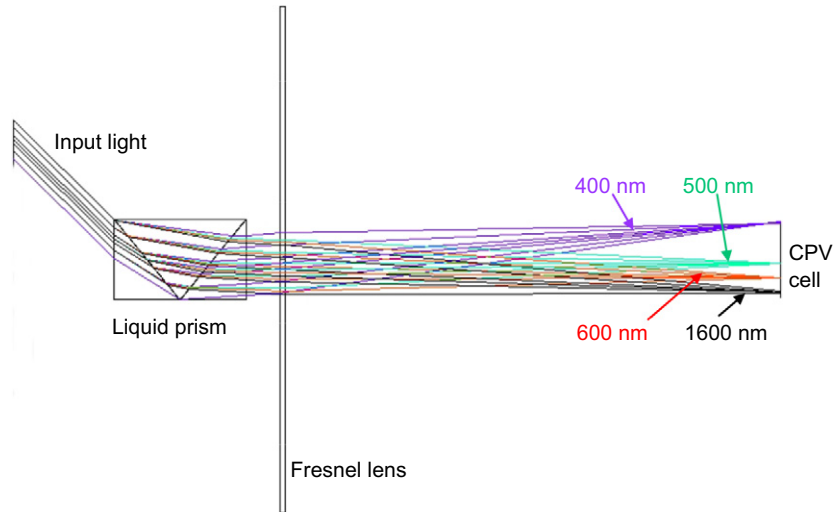


Fig. 7a. Optical layout of the solar concentration system in Zemax modeling.

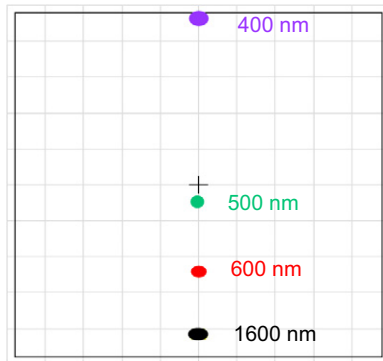


Fig. 7b. Footprint of the CPV cell of 16 mm × 16 mm.

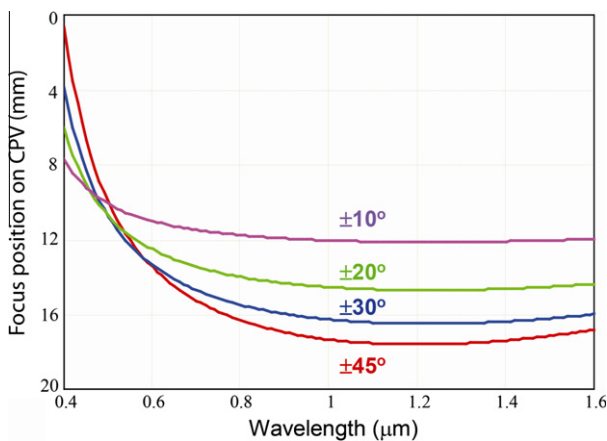


Fig. 8. CPV cell size requirements for different light incident angles.

efficiently and lead to a higher energy conversion efficiency (40–41%). However, the traditional solar trackers have mechanical moving parts that are expensive (sometimes even more expensive than the solar cells themselves) with a high maintenance cost (Mousazadeh et al., 2009). There-

fore, traditional CPV concentrator systems with bulky sizes are normally limited to field-level applications. In particular, due to their high power consumption and their heavy body, which raises reliability concerns, these CPV solar concentration systems are not suitable for residential rooftop applications (Luque and Andreev, 2007).

On the other hand, high-efficiency CPV solar cells are usually made with more pristine materials and complex processes, leading to a high fabrication cost (Neufeld et al., 2008). Typically, the cost of solar cells/modules is about 40–50% of the system costs. Our optofluidic concentrators can efficiently focus sunlight onto specially designed CPV solar cells with a high area reduction ratio ($>10^3$), thus reducing the number of CPV solar cells and $10 \times$ of the overall cost. Our analysis indicates that the optofluidic solar concentrators can generate ~ 3000 W on a 100 ft^2 rooftop. With the efficiency gains from the electro-optical concentrator, solar energy as a promising, clean, and renewable energy resource can be made more efficient and therefore affordable.

The optofluidic technology is unique and has clear distinctions from any of the existing solar concentration systems. The innovative features can be summarized as follows:

- *Electrowetting-controlled optofluidic concentrators with low power consumption.* Our electrowetting-based optofluidic solar system can achieve $10 \times$ power reduction in comparison to 300 W power consumption of the dual-axis motor-driven tracker system of SolFocus.
- *Adaptive solar tracking without mechanical moving parts.* This dual-axis optofluidic tracking system continuously modulates the liquid prism array to steer sunlight throughout the day for maximizing electricity generation (70% higher than a non-tracking PV system). This compact and low-profile configuration results in a highly efficient system suitable for rooftop installation.

Table 2
Comparison of three main approaches for solar concentration.

Parameters	PV solar panel ^a	CPV w/motorized tracking ^b	CPV w/liquid prism tracking ^c
Cell O-to-E efficiency	17%	40%	37–20%
Area size (for 100 W electric power)	5.3 ft ²	2.25 ft ²	3.16 ft ²
Weight (for 100 W electric power)	30 lb	40 lb ^d	34 lb ^e
Control power (for 100 W electric power)	0	2 W ^f	0.5 W ^g
Price (per 100 W electric power)	\$240	<\$300 (target)	<\$100 (target) ^h
Mechanical movement	No	Yes	No
Reliability	High	Low, motor life-time	High
Suitable for roof-top	Yes	No	Yes
Electric Power on 100 ft ² roof-top	1887 W	NA	3165 W

^a Suntech PV panel.

^b Solfocus CPV system.

^c Optofluidic solar concentration system.

^d 40% of PV solar panel weight + motor and frame.

^e 60% of PV solar panel weight + liquid prism.

^f Scaled down from a 1000 W CPV system.

^g Calculated power consumption of DC/AC controller.

^h Include manufacture cost.

- *Integration of optofluidic concentrators with a Fresnel lens to reduce the CPV cell size.* This arrangement will focus a large area of solar energy onto a smaller CPV cell with an area reduction ratio of $>10^3$, which is a significant improvement over state-of-the-art CPV systems. Solar concentration not only increases the electrical power obtained from each solar cell but also significantly reduces the cost of solar power since more electricity is obtained per solar cell, whereas fewer semiconductor materials are needed.
- *Using low-frequency square-wave AC signals to enhance electrowetting modules' reliability.* In contrast to DC voltage driving, the square-wave AC voltage avoids applying a high electric field over a long period to an electrode unit, which significantly increases the reliability and service life of optofluidic solar systems.
- *Improved heat dissipation and thermal management due to the distributed arrangement of CPV cells.* Exceptional performance and high reliability of the optofluidic concentration system can be ensured with proper thermal managements.

7. Conclusions

In this paper we introduce a high-performance optofluidic solar concentration system based on EWOD technique. The EWOD-controlled liquid prism module can, (a) actively control the liquid prism orientation with low power consumption, (b) agilely deflect and steer beam (sunlight) through the fluid–fluid interface, (c) adaptively track the beam source (sun) without any mechanical moving parts. We have fabricated a liquid prism module with an aperture size of 10 mm × 10 mm. With 1 wt% KCl and 1 wt% SDS added into DI water, the orientation of the water–silicone oil interface has been successfully modu-

lated between -45° and 45° that can deflect and steer sunlight within the incidence angle of -15° to 15° . Furthermore, we have described an optofluidic solar concentrator integrating electrowetting tracking and a static Fresnel lens condenser. We used Zemax to model the dispersion effect of the optofluidic concentration system. The numerical simulation indicates that optical fluid of low dispersion is critical to achieve high-density energy concentration on smaller CPV cells.

The theoretical performance and cost advantages of liquid prisms modules and optofluidic concentrators have been discussed in this work. In the optofluidic solar concentrator system, the EWOD-based self-tracking technology integrated with CPV cells will provide a highly efficient and performance-optimized energy harvesting system. In comparison with traditional silicon-based PV solar cells, our analysis shows that the EWOD-controlled optofluidic tracking technology will generate $\sim 70\%$ higher green energy with a 50% cost reduction. Importantly, the elimination of mechanical tracking hardware and quiet operation will allow extensive residential deployment of concentrated solar power. If successfully implemented, we believe this transformational optofluidic technology can make solar photovoltaic electric power generation systems not only economically competitive but also environmentally sustainable.

Acknowledgements

This work was supported by UNT startup fund, UMC startup fund and Advanced Research Projects Agency-Energy under contract No. DE-AR0000139.

References

- Antonio L. Luque and Viacheslav M. Andreev. 2007. Concentrator photovoltaics. Springer Series in Optical Sciences.

- Baker, K.A., Karp, J.H., Tremblay, E.J., Hallas, J.M., Ford, J.E., 2012. Reactive self-tracking solar concentrators: concept, design, and initial materials characterization. *Applied Optics* 51 (8), 1086–1094.
- Born, M., Wolf, E., 1999. *Principles of Optics*, 7th ed. Cambridge University Press.
- Cheng, J.-T., Chen, C.-L., 2010a. Adaptive chip cooling using electrowetting on coplanar control electrodes. *Nanoscale and Microscale Thermophysical Engineering* 14 (2), 63–74.
- Cheng, J.-T., Chen, C.-L., 2010b. Active thermal management of on-chip hot spots using EWOD-driven droplet microfluidics. *Experiments in Fluids* 49 (6), 1349–1357.
- Cheng, J.-T., Chen, C.-L., 2011. Adaptive beam tracking and steering via electrowetting-controlled liquid prism. *Applied Physics Letters* 99, 191108.
- Currie, M.J., Mapel, J.K., Heidel, T.D., Goffri, S., Baldo, M.A., 2008. High-efficiency organic solar concentrators for photovoltaics. *Science* 321 (5886), 226–228.
- Hayes, R.A., Feenstra, B.J., 2003. Video-speed electronic paper based on electrowetting. *Nature (London)* 425, 383–385.
- Hou, L., Smith, N.R., Heikenfeld, J., 2007. Electrowetting manipulation of any optical film. *Applied Physics Letters* 90, 251114.
- Huang, B.J., Ding, W.L., Huang, Y.C., 2011. Long-term field test of solar PV power generation using one-axis 3-position sun tracker. *Solar Energy* 85 (9), 1935–1944.
- Jones, T.B., 2005. An electromechanical interpretation of electrowetting. *Journal of Micromechanical and Microengineering* 15, 1184–1187.
- Kotsidas, P., Modi, V., Gordon, J.M., 2011. Nominally stationary high-concentration solar optics by gradient-index lenses. *Optics Express* 19 (3), 2325–2334.
- Kuiper, S., Hendriks, B.H.W., 2004. Variable-focus liquid lens for miniature cameras. *Applied Physics Letters* 85 (7), 1128–1130.
- Kurtz, S., 2011. Opportunities and challenges for development of a mature concentrating photovoltaic power industry. Technical Report NREL/TP-5200-43208.
- Lee, J., Moon, H., Fowler, J., Schoellhammer, T., Kim, C.J., 2002. Electrowetting and electrowetting-on-dielectric for microscale liquid handling. *Sensors and Actuators A – Physical* 95, 259–268.
- Mousazadeh, H., Keyhani, A., Javadi, A., Mobli, H., Abrinia, K., Sharifi, A., 2009. A review of principle and sun-tracking methods for maximizing solar systems output. *Renewable and Sustainable Energy Reviews* 13 (8), 1800–1818.
- Mugele, F., Baret, J.-C., 2005. Electrowetting: from basics to applications. *Journal of Physics: Condensed Matter* 17, R705–R774.
- Murade, C.U., Oh, J.M., van den Ende, D., Mugele, F., 2011. Electrowetting driven optical switch and tunable aperture. *Optics Express* 19 (16), 15525–15531.
- Neufeld, C.J., Toledo, N.G., Cruz, S.C., Iza, M., DenBaars, S.P., Mishra, U.K., 2008. High quantum efficiency InGaN/GaN solar cells with 2.95 eV band gap. *Applied Physics Letters* 93 (14), 143502.
- Pender, J.G. 2005. Motion-free tracking solar concentrator. US patent No: 6958868 B1.
- Roth, P., Georgiev, A., Boudinov, H., 2004. Design and construction of a system for sun-tracking. *Renewable Energy* 29 (3), 393–402.
- Rubio, F.R., Ortega, M.G., Gordillo, F., Lopez-Martinez, M., 2007. Application of new control strategy for sun tracking. *Energy Conversion and Management* 48 (7), 2174–2184.
- Smith, N.R., Abeysinghe, D.C., Haus, J.W., Heikenfeld, J., 2006. Agile wide-angle beam steering with electrowetting micropisms. *Optics Express* 14 (14), 6557–6563.
- Srinivasan, V., Pamula, V.K., Fair, R.B., 2004. An integrated digital microfluidic lab-on-a-chip for clinical diagnostics on human physiological fluids. *Lab on a Chip* 4, 310–315.